

PARALLEL SKELETONIZATION FOR INTEGRAL EQUATIONS IN EVOLVING MULTIPLY-CONNECTED DOMAINS

JOHN PAUL RYAN* AND ANIL DAMLE*

Abstract. This paper presents a general method for applying hierarchical matrix skeletonization factorizations to the numerical solution of boundary integral equations with possibly rank-deficient integral operators. Rank-deficient operators arise in boundary integral approaches to elliptic partial differential equations with multiple boundary components, such as in the case of multiple vesicles in a viscous fluid flow. Our generalized skeletonization factorization retains the locality property afforded by the “proxy point method,” and allows for a parallelized implementation where different processors work on different parts of the boundary simultaneously. Further, when the boundary undergoes local geometric perturbations (such as movement of an interior hole), the solution can be recomputed in logarithmic time with respect to the number of discretization nodes. We present an application that leverages a parallel implementation of skeletonization with updates in a shape optimization regime.

Key words. factorization updating, hierarchical factorizations, boundary integral equations, Stokes flow, shape optimization, fast direct solvers

AMS subject classifications. 65R20, 15A23, 76D07

1. Introduction. Consider the homogeneous boundary value problem

$$\begin{aligned} Lu(x) &= 0 & x \in \Omega \\ u(x) &= f(x) & x \in \Gamma \end{aligned}$$

where L is an elliptic differential operator, $f(x)$ is given Dirichlet data on the boundary Γ , and $u(x)$ is the desired solution in the interior domain Ω . Assuming sufficient smoothness of Γ and $f(x)$, the solution can often be efficiently numerically computed by considering the associated boundary integral equations:

$$(1.1) \quad u(x) = \int_{\Gamma} K_{\Omega}(x, y) \mu(y) d\Gamma(y) \quad x \in \Omega$$

$$(1.2) \quad \int_{\Gamma} K_{\Gamma}(x, y) \mu(y) d\Gamma(y) = f(x) \quad x \in \Gamma$$

where K_{Ω} and K_{Γ} are kernels related to the Green’s function and $\mu(x)$ is an intermediary function to be calculated via (1.2). This method requires only a discretization of the boundary, and allows for the computation of the solution at any point inside the domain without the need to discretize the entire domain.

Using K , μ , and f to denote the discretizations of the integral operator with kernel function $K_{\Gamma}(x, y)$, the unknown function $\mu(x)$, and the given function $f(x)$ respectively, the discretization of (1.2) is

$$(1.3) \quad K\mu = f.$$

Solving for μ given f requires a linear solve involving the dense matrix K , and for large discretizations of the boundary, general dense factorizations such as the LU

*Department of Computer Science, Cornell University, Ithaca, NY 14853
(johnryan@cs.cornell.edu, damle@cornell.edu).

decomposition can be prohibitively expensive. For this reason, it is advantageous to consider properties of K that enable more efficient factorizations.

In many cases, $K_\Gamma(x, y)$ satisfies an approximate separability condition:

$$(1.4) \quad K_\Gamma(x, y) \approx \sum_{i=1}^p u_i(x) v_i(y) \quad |x - y| > \gamma.$$

This property arises when $K_\Gamma(x, y) = K_\Gamma(x - y)$ and this function smoothly decays away from the origin, as is the case for many non-oscillatory Green's functions. For example, in Section 3.1 we examine the following boundary integral equation for computing viscous fluid flow velocities:

$$(1.5) \quad -\frac{1}{2}\mu(x) + \frac{1}{\pi} \int_\Gamma \frac{(x - y) \cdot n(y)}{\|x - y\|_2^4} (x - y) \otimes (x - y) \mu(y) d\Gamma(y) = f(x) \quad x \in \Gamma,$$

where $n(y)$ is the normal vector to the boundary Γ at y . Since the underlying kernel function satisfies (1.4), the discretized integral operator K will have numerically low rank off-diagonal blocks. In Section 2.2 we outline a hierarchical matrix factorization that leverages this property to approximate K by a product of easily invertible matrices [17, 30]. Given this approximate factorization of K , solving (1.3) can be done efficiently. Furthermore, as a direct method, this scheme is well suited to solve problems for many different right hand sides (for example, computing the solution in a fixed geometry for different boundary conditions).

When the boundary is multiply connected, *i.e.* $\Gamma = \Gamma_0 \cup \Gamma_1 \cup \dots \cup \Gamma_p$, the integral operator (and hence the matrix K) can become rank-deficient. In Section 3.1 we show how this degeneracy arises, and in Section 3.2 we develop a more general version of the skeletonization factorization applicable to these settings.

Throughout construction of the factorization, we compress off-diagonal blocks by decoupling sets of integration nodes based on analysis of kernel interactions. This compression is performed locally since it depends only on interactions with nearby integration nodes. The technique we use is known as the *proxy point method* [6, 27, 39, 18, 30, 7, 26, 17, 13, 11, 28, 4, 13, 38], and is described in Section 2.5. Local modifications to the underlying data Γ can be made without requiring full recomputation of the factorization of K . Further, the structure of the factorization persists following such modifications, and has all the benefits of a factorization computed from scratch. Section 2.7 reviews such a method for updating hierarchical skeletonization factorizations [28].

The fact that compression is performed locally and that updates to the factorization can be made quickly following geometric perturbations make this procedure particularly useful in optimization problems where solutions are calculated for many closely related boundaries. For example, this arises in objective function evaluation, search direction selection, line search, etc. In Section 4.3 we provide illustrative examples of this setting.

1.1. Background. The pioneering work in compressing discretizations of kernel matrices based on hierarchical rank structure is the development of the Fast Multipole Method (FMM) [15], which represents interactions between points at a distance by truncated multipole expansions. For problems where analytic expansions cannot be used, significant work has been done to develop kernel-independent methods [27, 39, 17, 18]. These methods perform compression algebraically by analyzing matrix entries directly (*i.e.* requiring samples of kernel interactions instead of analytic

expansions). The study of these techniques has involved a broad exploration of the purely algebraic properties of the matrices, instead of the underlying kernel function. In both the analytically and algebraically motivated regimes, these methods may be used to numerically solve linear systems, either via approximate direct solves or using them as preconditioners in iterative methods [24, 7, 26, 13, 10].

From a purely algebraic perspective, matrices displaying off-diagonal rank structure have been analyzed extensively and may fall into many different classes. Hierarchical off-diagonal low rank (HODLR) matrices satisfy the property that, given a tree-structured partitioning of the indices of the matrix, submatrices corresponding to different partitions of indices at the same level of the tree have rank less than k , a constant for the whole matrix. Hierarchically semi-separable (HSS) matrices are HODLR matrices with the additional property that each parent nodes basis can be constructed from those of its children (often referred to as a *nested bases*). \mathcal{H} (and \mathcal{H}^2) matrices [16, 5, 2] are like HODLR (and HSS) matrices except that 1) any partition tree (*i.e.* not just a binary partitioning) may be used to specify the rank-structure and 2) there is a so-called admissibility condition. Admissibility conditions dictate which pairs of partitions correspond to low-rank sub-matrices, such as those that are above a certain distance apart. Throughout this work we will assume our matrices satisfy the *weak admissibility condition*, *i.e.* all pairs of distinct partitions have low rank, and we refer the interested reader to [30, 8] for discussion on other admissibility conditions.

In settings where the solution is desired following small perturbations to the boundary geometry (for example, the rotation of a fin in a channel, or a modification to the shape of a wing on an airplane), several methods exist which efficiently solve related problems faster than completely refactoring the underlying matrix. One possibility is to treat the perturbations as low rank updates and apply the Sherman-Woodbury-Morrison formula [40], which takes advantage of the fact that the original factorization can be used for a fast linear solve. The advantage of this method is that no significant matrix factorizations need to be recomputed. On the other hand, this method will gradually slow as more low-rank updates are applied (say due to continuing changes to the boundary) and can encounter conditioning issues over time—for this reason in some settings is desirable to have an updating methodology that retains the form of the factorization while accumulating updates at each step. Minden, et al. [28] present a method for updating hierarchical skeletonizations which preserves the structure of the factorization at each updating step. This is the scheme that we appeal to here to deal with changes to domain boundaries. Importantly, here we focus on schemes applicable to integral equation formulations (other closely related, but distinct work, focuses on quadratures in this setting and related fast algorithms [37, 14]). However, rank-structured techniques are also often applicable to discretizations of differential operators [19] and in those settings alternative methodologies may be applicable [23].

An important application of rank-structured solvers to problems with changing boundary geometries is in viscous fluid flow simulations [4, 4, 35, 36]. For example, [35] uses a rank-structured solver for a microfluidic flow simulation, namely the deformation of inextensible vesicles in unbounded domains. Biros and Ying [3] have also demonstrated the applicability of these techniques in numerically solving unsteady Navier-Stokes equations. To our knowledge, no Stokes flow simulators exist that leverage a fast updating scheme to the rank-structured factorizations. Since the performance gains due to fast updating of the factorization accumulate over time, and applications can require 10^6 or more [35] linear solves, we consider the benefits of a

factorization updating scheme of substantial importance in this area.

1.2. Contribution. In this work we present a general formulation of a fast hierarchical matrix factorization applicable to boundary integral equations for simply or multiply connected domains. In addition, we demonstrate the ability of the factorization to be efficiently updated following changes to the boundary geometry. Previous work in this setting has experimented with small boundary or coefficient perturbations (*e.g.* adding a small bump to a simply connected boundary) that minimally affect the solution. The techniques we introduce allow for the deformation, movement, addition, and deletion of interior holes—changes to the problem that can have large effects on the solution throughout the domain. This is especially evident when we solve problems such as Stokes flow or steady-state heat with Neumann conditions in multiply-connected domains with moving interior holes. This represents a powerful new technique for the numerical solution of elliptic PDEs with many related boundary configurations and conditions.

We also present an implementation of the hierarchical factorization which parallelizes compression of nodes at each level of the quadtree. Arguing that this level of parallelism is most powerful in the initial factorization, we demonstrate how computational resources can be more efficiently allocated in problems where many updates to the factorization are required. This is the case in optimization settings where computing the ideal shape and/or size of interior holes is desired. Our work includes a novel demonstration of the benefits of hierarchical matrix factorization updating for such optimization problems, and this technique holds great promise for related time-dependent simulations, such as the simulation of vesicles in capillary flows. Our accompanying implementation allows for easy generation of multiply-connected boundaries and optimization given a user-specified objective function.

2. Preliminaries.

2.1. Notation. Throughout this manuscript we will use the matrix subscript notation K_{AB} to refer to the submatrix of K which contains the rows indexed by the index set A and the columns indexed by the index set B . We will refer to a submatrix which contains the rows indexed by A and all of the columns as $K_{A,:}$ and, analogously, $K_{:,B}$ is the submatrix which contains the columns indexed by B and all of the rows.

2.2. Hierarchical matrix factorization. The factorization we use is based on [17], and is applicable to matrices that arise from kernel discretizations where kernel interactions between well-separated subsets of points are numerically low-rank (*i.e.* the kernel function satisfies (1.4)). We begin by showing how to approximate such a kernel matrix as the product of easily invertible sparse matrices.

As a starting point, consider the set of points $B \cup F$ comprised of two disjoint subsets of points indexed by B and F with $|B| \ll |F|$ (think of B as corresponding to points inside a box and F as corresponding to many points outside the box). The matrix of kernel interactions may be written as

$$(2.1) \quad K = \begin{bmatrix} K_{BB} & K_{BF} \\ K_{FB} & K_{FF} \end{bmatrix}.$$

If our kernel satisfies (1.4)¹, then K_{FB} is numerically low-rank and we may construct

¹Specifically, the kernel should satisfy the *weak admissibility condition*, and we assume that it does throughout this work. If the kernel only satisfies the *strong admissibility condition*, then (2.1) would need blocks for non-low-rank interactions between points inside the box and points outside but nearby, see [30].

a low-rank approximation to K_{FB}

$$(2.2) \quad K_{FB} \approx WZ^T.$$

A popular choice in this setting is the interpolative decomposition [6]

$$W = K_{FS} \quad Z^T = [I \quad T],$$

where B is partitioned as

$$B = \{S \quad R\}$$

and we omit permutations of indices for the sake of exposition. In this partition, S and R stand for “skeleton” and “redundant” indices, respectively. The key idea is that we select the most important subset of indices S in B . We then represent interactions with points indexed by R as linear combinations of the important columns. Practically, S and T can be found via a column-pivoted QR factorization [12], and can be chosen so that (2.2) holds to any desired accuracy ε . We can use this factorization to decouple the redundant points by eliminating the FR and RF subblocks of K —this can be done by applying interpolation matrices on the left and right in the following manner

$$(2.3) \quad \begin{bmatrix} X_{RR} & X_{RS} & 0 \\ X_{SR} & K_{SS} & K_{SF} \\ 0 & K_{FS} & K_{FF} \end{bmatrix} \approx \begin{bmatrix} I & -T^T & 0 \\ 0 & I & 0 \\ 0 & 0 & I \end{bmatrix} \begin{bmatrix} K_{RR} & K_{RS} & K_{RF} \\ K_{SR} & K_{SS} & K_{SF} \\ K_{FR} & K_{FS} & K_{FF} \end{bmatrix} \begin{bmatrix} I & 0 & 0 \\ -T & I & 0 \\ 0 & 0 & I \end{bmatrix}.$$

We use X to denote a matrix block that has been modified, and we have assumed K is symmetric (Section 2.4 discusses nonsymmetric kernels). We may now use block Gaussian elimination to decouple R from the rest of the matrix via

$$(2.4) \quad \begin{bmatrix} X'_{RR} & 0 & 0 \\ 0 & X_{SS} & K_{SF} \\ 0 & K_{FS} & K_{FF} \end{bmatrix} = G_L \begin{bmatrix} X_{RR} & X_{RS} & 0 \\ X_{SR} & K_{SS} & K_{SF} \\ 0 & K_{FS} & K_{FF} \end{bmatrix} G_R,$$

where

$$(2.5) \quad G_L = \begin{bmatrix} I & 0 & 0 \\ -X_{SR}X_{RR}^{-1} & I & 0 \\ 0 & 0 & I \end{bmatrix} \quad G_R = \begin{bmatrix} I & -X_{RR}^{-1}X_{RS} & 0 \\ 0 & I & 0 \\ 0 & 0 & I \end{bmatrix}.$$

In summary, by applying easily invertible sparse matrices on the left and right of K we construct a sparser matrix. Importantly, the K_{FF} block remains unchanged and it may be further compressed in the same way. Ultimately, our goal is to iteratively apply this method to sparsify K as much as possible. To that end, we must discuss how to iteratively choose the index sets B and F .

2.3. Interaction matrices and domain decompositions. Common sources of hierarchical matrices are problems where entries K_{ij} are kernel interactions between points x_i and x_j in space. Some examples include covariance matrices in Gaussian processes and kernel matrices in boundary integral equation discretizations [29, 25]. In these settings, we form a tree decomposition of the domain that reveals compressible subblocks based on relationships between tree nodes.

Suppose we wish to factor the interaction matrix of a set of points x_1, \dots, x_N along a circle (see Fig. 1). We first form an adaptive quadtree decomposition of the domain, such that the leaves of our tree contain no more than a prescribed constant number

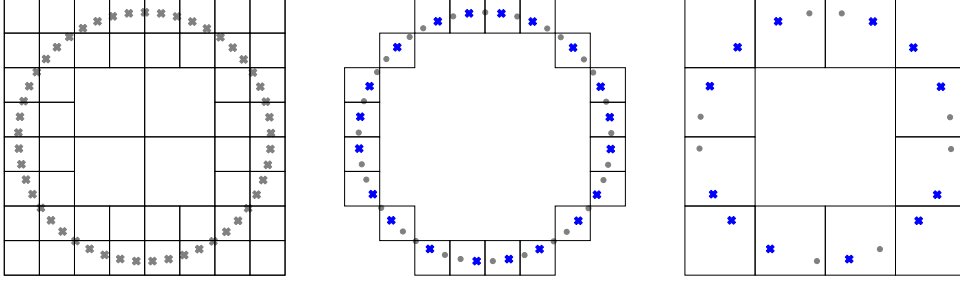


FIG. 1. Left: we start by building an adaptive quadtree decomposition of the domain where the leaf level nodes contain fewer than some prescribed amount of points (grey x 's). Center: focusing first on the nonempty leaf nodes with points inside, we perform the compression (2.7) for every box at the leaf level, partitioning the points in each box into skeleton points (blue x 's) and redundant points (grey circles). Right: we continue compression by moving up one level in the tree and considering only the skeleton points from the previous level. We then perform the same compression procedure as before for the new boxes, thereby further shrinking the total number of skeleton points. Note that the above figures are purely illustrative—in reality, the ratio of redundant points to skeleton points is typically far greater.

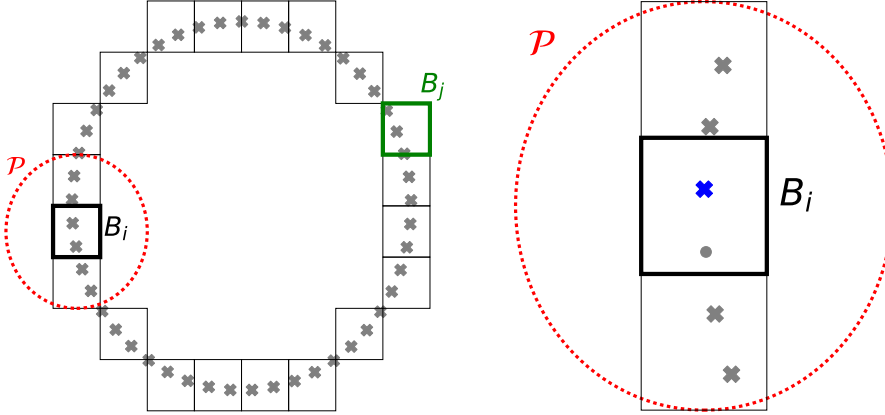


FIG. 2. Left: for many kernels, the interactions between points in a box B (bold) and distant points can be well approximated by considering interactions between the interior points and points on a “proxy” circle \mathcal{P} (red). Section 2.5 describes how to compute compression matrices for this box using only points on and inside of \mathcal{P} . Right: the only information needed to perform compression for a box B are its points’ interactions with nearby points and with points along a proxy circle. Importantly, points in distant boxes (for example, in the green box B_j in the left figure) can be added, deleted, or moved around, and the compression matrices and skeleton/redundant partitions for B are still valid.

of points. Working first at the leaf level of the tree, we let B_i be the set of all indices corresponding to points in the i th leaf box. We then let F_i be the set of all indices of points outside of the i th leaf box so that we may compress

$$(2.6) \quad K = \begin{bmatrix} K_{B_i B_i} & K_{B_i F_i} \\ K_{F_i B_i} & K_{F_i F_i} \end{bmatrix}$$

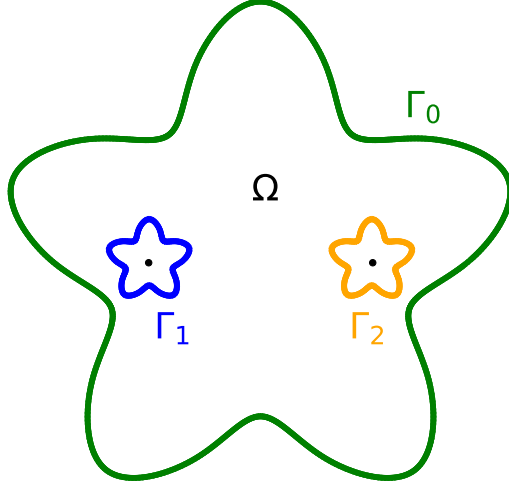


FIG. 3. *Multiply-connected boundary. The dots inside Γ_1 and Γ_2 represent points (c_1 and c_2 respectively) outside the domain Ω used in the construction of the Stokeslets and rotlets in Section 3.1.*

in the following way

$$(2.7) \quad \begin{bmatrix} X_{R_i R_i} & 0 & 0 \\ 0 & X_{S_i S_i} & K_{S_i F_i} \\ 0 & K_{F_i S_i} & K_{F_i F_i} \end{bmatrix} \approx U_i K V_i,$$

where the U_i and V_i matrices are products of the block unitriangular compression matrices in (2.3) and (2.5). We will use B_i to refer both to the index set and its corresponding box in the quadtree, and we will refer to the above procedure as “compressing box B_i .” In practice we do not explicitly form U_i and V_i but instead apply the constituent matrices in sequence taking advantage of their block unitriangular structure.

We may then consider $K_{F_i F_i}$ and compress every other box on this level, yielding

$$(2.8) \quad \begin{bmatrix} X_{R_1 R_1} & 0 & 0 & 0 & 0 & 0 & 0 \\ 0 & \ddots & 0 & 0 & 0 & 0 & 0 \\ 0 & 0 & X_{R_m R_m} & 0 & 0 & 0 & 0 \\ 0 & 0 & 0 & X_{S_1 S_1} & K_{S_1 S_2} & \dots & K_{S_1 S_m} \\ 0 & 0 & 0 & K_{S_2 S_1} & X_{S_2 S_2} & \dots & K_{S_2 S_m} \\ 0 & 0 & 0 & \vdots & \vdots & \ddots & \vdots \\ 0 & 0 & 0 & K_{S_m S_1} & K_{S_m S_2} & \dots & X_{S_m S_m} \end{bmatrix} \approx U^{(l)} K V^{(l)},$$

where l is the level number (in (2.8) we have $l = L$ where L is the depth of the tree), m is the number of boxes at level l and

$$(2.9) \quad U^{(l)} = \prod_{i=1}^m U_{m-i+1} \quad V^{(l)} = \prod_{i=1}^m V_i.$$

The bottom-right block of (2.8) is an interaction matrix between the skeleton points that haven't yet been compressed after level l , with some modifications to the diagonal blocks. Since the process of (2.6)-(2.7) relies only on the compressibility of the off-diagonal blocks, we may recurse on this set of skeleton points by moving up a level in the quadtree (see Fig. 1, right).

Recurring until there are no more far-field interactions to compress (*i.e.* reaching the root of the quadtree) yields the factorization

$$(2.10) \quad X_D := \begin{bmatrix} X_{R_1 R_1} & 0 & 0 & 0 \\ 0 & \ddots & 0 & 0 \\ 0 & 0 & X_{R_n R_n} & 0 \\ 0 & 0 & 0 & X_{SS} \end{bmatrix} \approx UKV,$$

where

$$(2.11) \quad U = \prod_{l=1}^L U^{(L-l+1)} \quad V = \prod_{l=1}^L V^{(l)}.$$

In summary, we have produced an approximate factorization

$$K \approx \hat{K} = U^{-1} X_D V^{-1},$$

and an approximate solution to $Kx = b$ may be computed via

$$(2.12) \quad x = K^{-1}b \approx \hat{K}^{-1}b = V X_D^{-1} U b,$$

where factorizations of blocks on the diagonal X_D are computed at factor time, not solve time. The overall accuracy of these approximations is closely related to the prescribed accuracy of the interpolative decompositions, see [11, 17, 18, 26] for further discussion. Notably, the ability to control the accuracy of this factorization also allows for the construction of a good preconditioner for an iterative method [33].

In practice, the dominant cost in (2.12) is often factoring the dense subblock X_{SS} of X_D . As a result, the overall cost of the factorization is cubic in the final number of skeleton indices. Under mild assumptions on the growth of skeleton points per level a more detailed complexity analysis can be done—[18] shows $\mathcal{O}(n)$ scaling of the factorization based on the observation that skeleton points tend to cluster near box interfaces. This linear scaling, which we demonstrate empirically in Section 4.1, will require the widely-used “proxy point method” to avoid formation of large off-diagonal blocks, which we discuss in Section 2.5.

2.4. Nonsymmetric matrices. In Section 2.2, we only use symmetry of K to compress K_{FB} and K_{BF} with the same T matrix. If K is not symmetric, we can still find index sets S and R and a compression matrix T by computing the interpolative decomposition

$$\begin{bmatrix} K_{FS} \\ K_{SF}^T \end{bmatrix} T \approx \begin{bmatrix} K_{FR} \\ K_{RF}^T \end{bmatrix}.$$

This procedure is simple to implement, works well in practice, and avoids having to keep track of distinct skeleton sets and interpolation matrices for each direction.

2.5. Proxy circle trick. A prohibitively costly component of the compression scheme in Section 2.2 is the formation and column-pivoted QR factorization of K_{FB} . If K comes from a boundary integral equation corresponding to an elliptic PDE with constant coefficients, we can apply the following widely used remedy [6, 27, 39, 18, 30, 7, 26, 17, 13, 11, 28, 4, 13, 38]. Consider drawing a circle \mathcal{P} around box B (see Figure 2, left) and partitioning the index set F into $F = F_{int} \cup F_{ext}$, where F_{int} are indices corresponding to points inside \mathcal{P} and F_{ext} are outside. We can then write

$$(2.13) \quad K_{FB} = \begin{bmatrix} K_{F_{int}B} \\ K_{F_{ext}B} \end{bmatrix} \approx \begin{bmatrix} I & 0 \\ 0 & M_{F_{ext}\mathcal{P}} \end{bmatrix} \begin{bmatrix} K_{F_{int}B} \\ K_{\mathcal{P}B} \end{bmatrix}$$

where the approximate representation $K_{F_{ext}B} \approx M_{F_{ext}\mathcal{P}} K_{\mathcal{P}B}$ is derived from discretizing

$$(2.14) \quad K(x - z) = \int_{\mathcal{P}} K(x - y) \phi(y) dy.$$

The existence of this representation follows from Green's theorem (see [18] for more details). Instead of performing a costly compression of K_{FB} , we compress the asymptotically smaller matrix on the RHS of (2.13)

$$(2.15) \quad \begin{bmatrix} K_{F_{int}B} \\ K_{\mathcal{P}B} \end{bmatrix} \approx \begin{bmatrix} K_{F_{int}S} \\ K_{\mathcal{P}S} \end{bmatrix} \begin{bmatrix} I & T \end{bmatrix}.$$

Using the interpolative decomposition (2.15) in conjunction with (2.13), we see that the index set S and interpolation matrix T also compress the matrix K_{FB} . The additional error we incur from the integral discretization is related to the size of the discretization and the behavior of the kernel. In most cases, we fix the number of discretization nodes on \mathcal{P} so that $|\mathcal{P}| \ll |F_{ext}|$ and the integral discretization error is negligible compared to the ID error.

Although the above is sufficient for this work, we note that the use of proxy points can be extended to more general kernels. For example, common kernels arising when working with kernelized Gaussian processes necessitate the use of a proxy annulus [29]. Xing and Chow [38] present an algorithmic procedure for selecting proxy points for a given kernel.

2.6. Parallelization. Consider the impact of the order in which we compress boxes on a level. After compressing the first box on the leaf level, the factorization looks like

$$(2.16) \quad \begin{bmatrix} X_{RR} & 0 & 0 \\ 0 & X_{SS} & K_{SF} \\ 0 & K_{FS} & K_{FF} \end{bmatrix} = U \begin{bmatrix} K_{RR} & K_{RS} & K_{RF} \\ K_{SR} & K_{SS} & K_{SF} \\ K_{FR} & K_{FS} & K_{FF} \end{bmatrix} V.$$

In particular the data required to compress subsequent boxes at the leaf level is nearly the same. The only exception is the introduction of zeros in the K_{RF} and K_{FR} blocks.

This observation allows us to compress every box on a level in parallel. To see this, notice that given T from an interpolative decomposition of the dense matrix

$$\begin{bmatrix} A \\ B \end{bmatrix} \approx \begin{bmatrix} A_{skel} \\ B_{skel} \end{bmatrix} \begin{bmatrix} I & T \end{bmatrix},$$

the same T also satisfies

$$\begin{bmatrix} A \\ 0 \end{bmatrix} \approx \begin{bmatrix} A_{skel} \\ 0 \end{bmatrix} \begin{bmatrix} I & T \end{bmatrix}.$$

Consequently, we may compress all boxes on a given level in parallel (neglecting to propagate the zeros in the LHS of (2.16) until moving onto the next level) and still achieve an accurate factorization.

A trade-off is that there may be less compression when parallelizing this way since the skeleton sets are found by solving slightly larger interpolation problems than necessary. Fortunately, use of the proxy surface mitigates this concern—zeros introduced outside the proxy surface of a given box have no effect on its compression (see Fig. 2, right). Furthermore, in practice the speedup due to parallelizing an entire level outweighs the cost due to marginally less efficient compression of boxes.

We make note of one further opportunity for parallelism that exists regardless of whether or not the above parallel compression scheme is employed during factorization. Consider applying $V^{(l)}$ in (2.9) to a vector

$$V^{(l)}x = \left(\prod_{i=1}^m V_i \right) x.$$

The block unitriangular matrices V_i act on disjoint sets of components of x (in particular, V_i acts only on those x_j where $j \in B_i$), and hence can be applied in parallel. The application of $U^{(l)}$ can also be parallelized for the same reason, as can X_D as a block diagonal matrix, and also the inverses of these matrices.

2.7. Fast updating after perturbation. One major benefit of this form of factorization is that if discretization nodes are added, deleted, or moved around in a small area of the domain (such that relatively few of the leaf-node boxes are affected) the factorization can be updated with relative ease while maintaining the same structure.

Suppose that some points in the green box of Fig. 2, left, are perturbed. Due to the locality afforded by the proxy trick, compression of the bold-faced box B_i is completely unaffected. In other words, compression matrices associated with B_i (X_{R_i, R_i} , X_{S_i, S_i} , U_i and V_i) will be the same before and after modifications to points inside the green box B_j , and hence we needn't recompute them. Similarly, corresponding blocks along the diagonal of X_D^{-1} in (2.12) are unchanged, and their LU factorizations may be reused.

We omit the details here, but carefully considering the propagation of influence of modifications to the points yields a rule for which boxes in the tree require recompression, and how to update the underlying quadtree [28]. Moreover, [28] shows that the complexity of this updating scheme is linear in the number of perturbed points.

An important impact of the locality of this updating scheme is that there is less opportunity for parallelism due to the relatively small number of boxes needing recompression per level. We experimentally explore the consequences of these details in Section 4.3.

3. Problem description. The procedures described in Section 2 are applicable to a broad range of problems in which certain kernel functions arise. In this work, we mainly focus on their applicability to the computation of steady viscous fluid flow given velocity boundary conditions in a 2D domain. This requires developing a boundary integral formulation of the relevant Stokes equations. We then use these techniques to numerically solve a discretized version of the problem. In this section

we describe the relevant differential equations and their representation as integral equations on the boundary.

3.1. Stokes equations. The Stokes equations

$$(3.1) \quad -\Delta u(x) + \nabla p(x) = 0, \quad \nabla \cdot u(x) = 0,$$

describe steady-state fluid velocity $u(x) \in \mathbb{R}^2$ and pressure $p(x) \in \mathbb{R}$ in incompressible flows where inertial forces are very small compared to viscous forces. They come from taking the limit of the non-dimensionalized Navier-Stokes equations as the Reynold's number vanishes.

Consider the interior boundary value problem with boundary Γ and corresponding Dirichlet data

$$(3.2) \quad u(x) = f(x), \quad x \in \Gamma.$$

Due to the linearity of (3.1), we may (under mild assumptions, see [20] Section 2.3) solve for the fluid velocity $u(x)$ on the interior Ω of Γ by solving a set of corresponding boundary integral equations.

The boundary integral approach represents the solution inside the domain as a boundary integral of some *single* or *double layer potential*. In electrostatics this is analogous to representing an electric field as an integral of a charge (single layer) or dipole (double layer) density on a surface. Following [4, 32, 34] we use the *stresslet*² as our kernel function, and the resulting boundary integral is

$$(3.3) \quad u(x) = \frac{1}{\pi} \int_{\Gamma} \frac{(x-y) \cdot n(y)}{\|x-y\|_2^4} (x-y) \otimes (x-y) \mu(y) d\Gamma(y) \quad x \in \Omega.$$

Plugging (3.3) into (3.2) and taking the limit as x approaches a point on Γ results in

$$(3.4) \quad f(x) = -\frac{1}{2}\mu(x) + \frac{1}{\pi} \int_{\Gamma} \frac{(x-y) \cdot n(y)}{\|x-y\|_2^4} (x-y) \otimes (x-y) \mu(y) d\Gamma(y) \quad x \in \Gamma.$$

The $-\frac{1}{2}\mu(x)$ is the result of a jump relation of the double layer potential as it approaches the boundary.

Solutions to (3.4) exist but are not unique—the linear operator on the RHS has a one-dimensional null-space corresponding to the constraint that the net flux of fluid across Γ be zero. We eliminate the null-space by adding

$$(3.5) \quad \int_{\Gamma} n(x) \otimes n(y) \mu(y) dy.$$

to the RHS of (3.4) [32, 4].

When the domain is multiply connected (*i.e.* $\Gamma = \Gamma_0 \cup \Gamma_1 \cup \dots \cup \Gamma_p$, see Figure 3), (3.3) cannot represent flows resulting from singularities in the interiors of the holes in the domain (see [34] for further discussion on this). Following [32] the *Stokeslet* and *rotlet* are defined as³

$$(3.6) \quad S_i \alpha_i := \frac{1}{4\pi} \left(\ln \frac{1}{\|x - c_i\|_2} + \frac{(x - c_i) \otimes (x - c_i)}{\|x - c_i\|_2^2} \right) \alpha_i,$$

²The stresslet is the symmetric part of the first moment of force for the Stokes equations.

³The Stokeslet is the zeroth moment of force, and the rotlet is the antisymmetric part of the first moment of force for the Stokes equations.

$$(3.7) \quad R_i \beta_i := \frac{1}{4\pi \|x - c_i\|_2^2} (x - c_i)^\perp \beta_i.$$

The Stokeslet represents the free-space solution of (3.1) at x due to a point force at c_i , and the rotlet represents the solution at x due to a point torque at c_i . Letting c_1, \dots, c_p be points on the interiors of $\Gamma_1, \dots, \Gamma_p$ respectively (so that $c_i \notin \Omega$, see dots in Figure 3), and letting D represent the integral operator in (3.3) we have the concise representation

$$(3.8) \quad u = D\mu + S\alpha + R\beta := D\mu + \sum_{i=1}^p S_i \alpha_i + \sum_{i=1}^p R_i \beta_i.$$

Any solution $u(x)$ of (3.1) can be represented by (3.8).

For conciseness we summarize the equations for u and f as

$$(3.9) \quad [u] = \begin{bmatrix} D & H \end{bmatrix} \begin{bmatrix} \mu \\ \lambda \end{bmatrix},$$

$$(3.10) \quad [f] = \begin{bmatrix} -\frac{1}{2}I + D + N & H \end{bmatrix} \begin{bmatrix} \mu \\ \lambda \end{bmatrix}$$

where

$$(3.11) \quad H := \begin{bmatrix} S & R \end{bmatrix} \quad \lambda := \begin{bmatrix} \alpha \\ \beta \end{bmatrix}.$$

Unfortunately, (3.10) is undetermined as

$$(3.12) \quad \left(-\frac{1}{2}I + D + N \right) \Psi = 0$$

for the matrix Ψ representing the null-space

$$(3.13) \quad \Psi = \begin{bmatrix} \psi_1^{(1)} & \psi_1^{(2)} & \psi_1^{(3)} & \dots & \psi_p^{(1)} & \psi_p^{(2)} & \psi_p^{(3)} \end{bmatrix}$$

$$(3.14) \quad \psi_i^{(1)} = \begin{cases} e_1^T & x \in \Gamma_i \\ [0 \quad 0]^T & x \in \Gamma \setminus \Gamma_i \end{cases} \quad \psi_i^{(2)} = \begin{cases} e_2^T & x \in \Gamma_i \\ [0 \quad 0]^T & x \in \Gamma \setminus \Gamma_i \end{cases}$$

$$(3.15) \quad \psi_i^{(3)} = \begin{cases} (x^\perp)^T & x \in \Gamma_i \\ [0 \quad 0]^T & x \in \Gamma \setminus \Gamma_i \end{cases}.$$

We address this degeneracy by augmenting as [32, 4]

$$(3.16) \quad \begin{bmatrix} f \\ 0 \end{bmatrix} = \begin{bmatrix} -\frac{1}{2}I + D + N & H \\ \Psi^T & -I \end{bmatrix} \begin{bmatrix} \mu \\ \lambda \end{bmatrix}.$$

Note that we are taking the adjoint of Ψ in the functional sense, and so $\Psi^T \mu$ is an integral.

The unique solution to (3.16) may be computed and plugged into (3.9) to find the unique solution to the boundary value problem (3.1)-(3.2).

3.2. Skeletonization of a hierarchical submatrix. The matrix in (3.16) is not the discretization of a kernel function satisfying (1.4), and hence the tools of Section 2.2 are not directly applicable. To generalize skeletonization to this setting, we factor the top-left block (which *is* the discretization of a kernel satisfying (1.4)) and apply the resulting interpolation matrices to H and Ψ^T in the following manner

$$(3.17) \quad \begin{bmatrix} -\frac{1}{2}I + D + N & H \\ \Psi^T & -I \end{bmatrix} \approx \begin{bmatrix} U^{-1} & 0 \\ 0 & I \end{bmatrix} \begin{bmatrix} X_D & UH \\ \Psi^T V & -I \end{bmatrix} \begin{bmatrix} V^{-1} & 0 \\ 0 & I \end{bmatrix}.$$

Inverting both sides of (3.17) and plugging into (3.16) and subsequently (3.9) yields

$$(3.18) \quad u \approx [D \ H] \begin{bmatrix} V & 0 \\ 0 & I \end{bmatrix} \begin{bmatrix} X_D & UH \\ \Psi^T V & -I \end{bmatrix}^{-1} \begin{bmatrix} U & 0 \\ 0 & I \end{bmatrix} \begin{bmatrix} f \\ 0 \end{bmatrix}.$$

To perform the necessary linear solve, a naïve attempt might try and take advantage of the block diagonal structure of X_D and perform block Gaussian elimination with Schur's complement

$$M_{Schur} = -I - \Psi^T V X_D^{-1} UH.$$

Unfortunately, the degeneracy of $-\frac{1}{2}I + D + N$ (see (3.12)) experimentally manifests as poor conditioning of the subblock⁴ X_{SS} of X_D , thereby rendering a linear solve with X_D infeasible. To address this, we consider an alternative partitioning of the skeletonized matrix

$$(3.19) \quad \begin{bmatrix} X_D & UH \\ \Psi^T V & -I \end{bmatrix} = \left[\begin{array}{ccc|cc} X_{R_1 R_1} & 0 & 0 & & \\ 0 & \ddots & 0 & 0 & (UH)_{R,:} \\ 0 & 0 & X_{R_n R_n} & & \\ \hline & 0 & & X_{SS} & (UH)_{S,:} \\ & (\Psi^T V)_{:,R} & & (\Psi^T V)_{:,S} & -I \end{array} \right].$$

In this case the diagonal blocks are nonsingular, and we may safely use block Gaussian elimination to solve the linear system. Since in most cases we have $p \ll |S|$, the cost of factoring the Schur's complement is effectively still cubic in $|S|$.

We also note that the updating scheme from Section 2.7 naturally generalizes to solving (3.18) using the partitioning in (3.19). As before, we avoid unnecessarily recomputing and refactoring subblocks of X_D , U , and V corresponding to boxes far from the perturbation. Further, interior holes can be added or deleted with ease when using an adaptive quadtree—the dominant cost continues to be the inversion of the updated Schur's complement.

4. Numerical results. We implemented the factorization routine in C++ using Intel's Math Kernel Library for matrix operations and OpenMP for parallelization. The code and experiments are available at <https://github.com/jpryan1/kern-interp>. All testing was conducted on a workstation with a 3.6 GHz quad-core Intel Core i7 CPU and 32 GB of RAM. All timing plots display average times over three runs of the relevant computation. Below we illustrate the program's performance with several example problems chosen to demonstrate the algorithm's strengths, and the benefits of parallelism and factorization updates in optimization settings. We use four cores and parallelize according to Section 2.6 for the first two experiments, and then vary our parallelization scheme in the optimization experiments.

⁴In our experiments we have not observed poor conditioning of an X_{RR} block, but if this occurs, the ill-conditioned subblocks can be grouped with X_{SS} in the bottom-right block of (3.19).

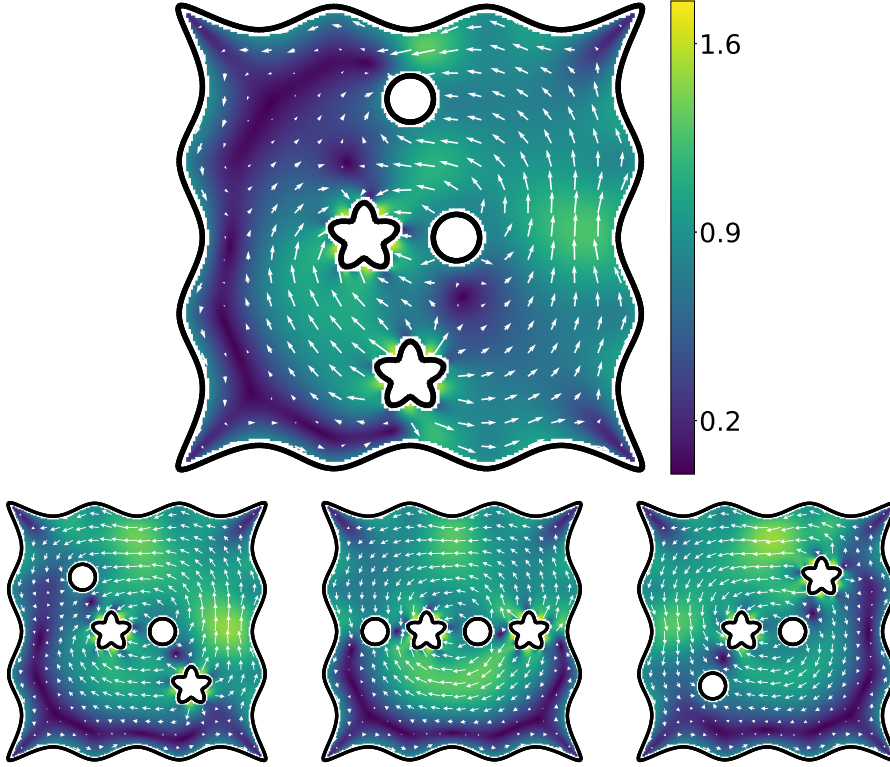


FIG. 4. Stokesian flow velocities in a multiply connected domain. The solution is quickly recalculated after repositioning the inner holes. We discretize the boundary using 4,096 integration nodes, with $2/3$ of them on the outer boundary and $1/12$ on each of the interior holes, rounded as appropriate. The solution is evaluated throughout the domain, though we intentionally avoid evaluation near the boundaries as more sophisticated techniques are required [22].

4.1. Stokes flow with moving fluid sources/sinks. In our first experiment (visualized in Figure 4), we create a smooth squiggly outer boundary via cubic spline interpolation of 24 prescribed spline knots (note that this enforces smoothness of the boundary). On the inside are four interior holes—two are circles and two are starfish curves, again created as cubic spline interpolations of arranged spline points. For boundary conditions, we assign the following Dirichlet data:

- The outer boundary has unit-length counter-clockwise tangential flow.
- One starfish and one circle each act as “sources,” with unit-length normal flow into the domain.
- The other two holes act as “sinks,” with unit-length normal flow into the hole.

Notice that the above Dirichlet data satisfies the consistency condition coming from incompressibility. Fig. 5 shows that factoring and solving the associated linear system scales linearly with the number of quadrature nodes on the boundary. Note that in Figures 5 and 6 that N points with p boundaries in a Stokes flow experiment result in a matrix of size $2N + 3p$ (see (3.16)).

After the initial factorization, the outermost interior holes are repositioned to nearby locations. Following this change to the boundary, we update the factorization

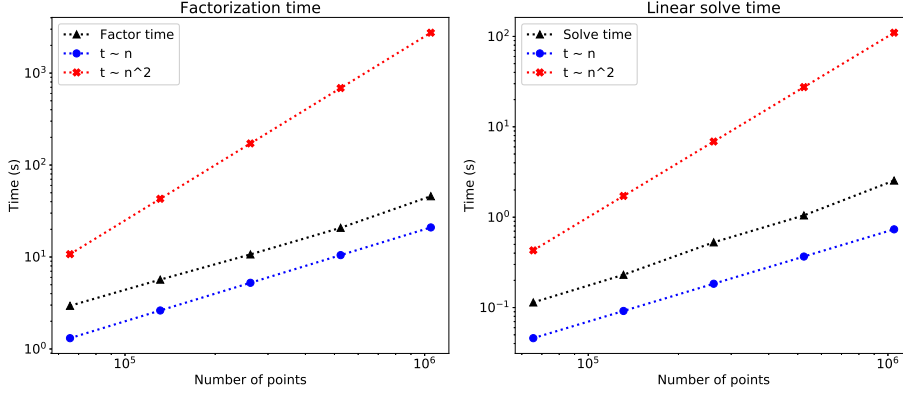


FIG. 5. Both factoring and solving demonstrate linear scaling in the number of discretization points along the boundary.

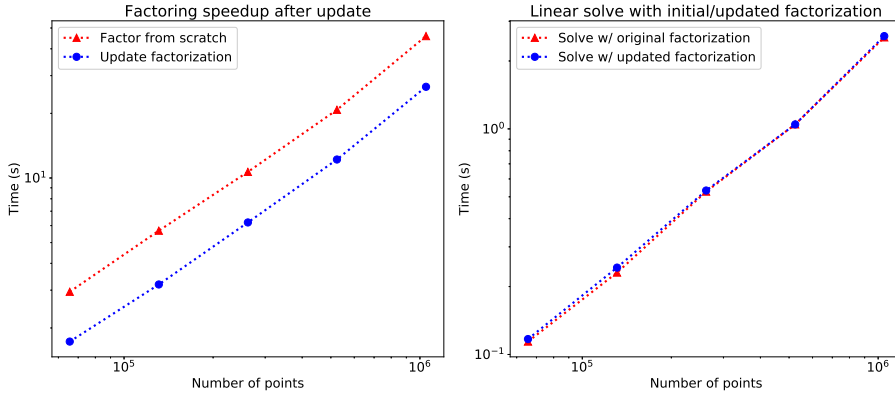


FIG. 6. Left: The updating scheme of Section 2.7 results in a 2x speedup in the factorization of the linear system for Ex. 1. Right: Using the updating scheme has no effect on the cost of the linear solve.

based on the perturbations to the discretization nodes. In Figure 6 we see that updating the factorization based on the technique in Section 2.7 results in a 2x speedup over recomputing the factorization from scratch. Figure 6 also shows that the cost of computing a linear solve in the perturbed geometry is effectively the same regardless of whether that factorizations is from scratch or from an update.

4.2. Stokes flow through a channel with many moving interior holes.

In our second experiment (zoomed-in visualization in Fig. 7), we simulate Stokes flow in a channel with ten interior circular holes. The outer boundary is a long rectangle with rounded corners, and the boundary conditions are again Dirichlet data. We prescribe horizontal unit-length velocities on the left and right walls, and zero velocities (no slip) on the top and bottom walls and on the interior circles.

To illustrate the power of maintaining the same factorization structure across updates, we perform one hundred changes to the positions of the interior holes. Table 1 shows that, after initial factorization, subsequent factorizations (for different problem geometries) require significantly less time to compute by using the updating scheme.

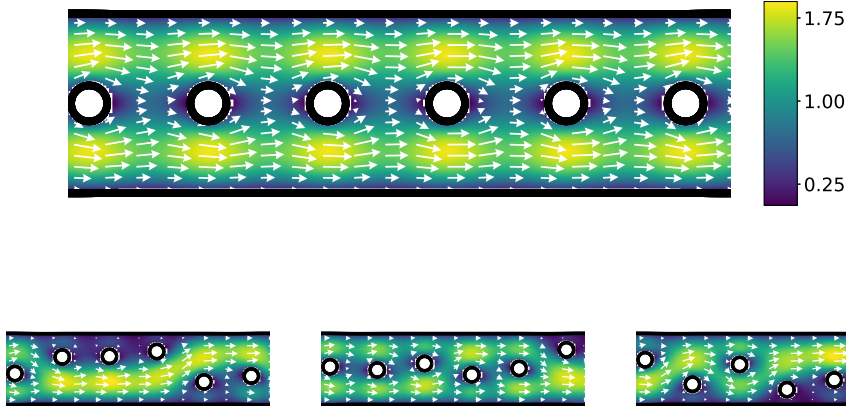


FIG. 7. Stokes flow solution for a channel-like outer boundary with interior holes. We initially construct a factorization for the top geometry, and use the updating scheme to develop factorizations for the bottom geometries. We discretize the boundary using 4,096 integration nodes, with $3/4$ of the integration nodes on the outer boundary and $1/32$ on each of the eight interior boundaries, rounded as appropriate. The above image is zoomed in to show the flow in detail.

Furthermore, the time required to update the factorization remains relatively stable.

TABLE 1

Cost of initial factorization and subsequent updates, along with statistics for factorization update times. For this experiment, we discretize the boundary using 131,072 integration nodes.

Initial fact.	1st update	100th update	Update time μ	Update time σ
5.03 s	1.54 s	1.58 s	1.52 s	0.04 s

As described at the end of Section 2.7, the speedup due to parallel compression of boxes on each level is mostly seen in the initial factorization, with the factorization updates benefiting relatively less. One way to maintain efficient processor usage is to compute the initial factorization in parallel as described in Section 2.6, and then compute distinct updates each on independent processors. This is particularly beneficial for problems in which we know a priori a large number of related geometries in which we would like to know the solution. An example of this is exploring a solution landscape locally in an optimization problem. We explore this setting in the following experiments.

4.3. Shape optimization.

4.3.1. Optimizing heat source/sink placement. In this experiment (visualized in Fig. 8) we calculate steady-state temperature distributions given Neumann boundary conditions, *i.e.* we solve Laplace's equation

$$\Delta u(x) = 0 \quad x \in \Omega$$

for many geometries. Our goal will be to maximize an objective function of the solution to be discussed later. The setup is similar to the Stokes problems, with the following exceptions:



FIG. 8. Steady state heat distribution given flux conditions on the boundaries. We discretize the boundary using 4,096 integration nodes, with $2/3$ of the integration nodes on the outer boundary and $1/6$ on each of the two interior boundaries, rounded as appropriate. Visualized is the geometry with $\theta_1 = 0$ and $\theta_2 = \pi$.

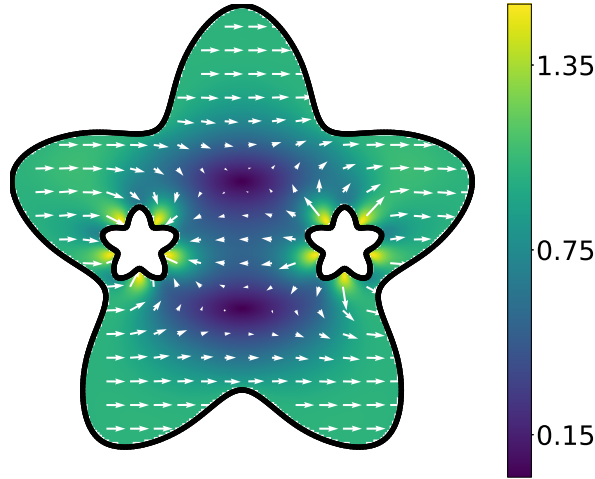


FIG. 9. Stokes flow inside the domain given prescribed velocities along the boundary. We discretize the boundary using 4,096 integration nodes, with $2/3$ of the integration nodes on the outer boundary and $1/6$ on each of the two interior boundaries, rounded as appropriate. Visualized is the geometry with $\theta_1 = 0$ and $\theta_2 = \pi$.

- Equation (3.9) becomes

$$u = S\mu$$

where S is the *single layer potential* for the 2D Laplace problem defined as

$$S\mu := - \int_{\Gamma} \frac{1}{2\pi} \log |x - y| \mu(y) dy.$$

- Equation (3.16) becomes

$$f = \left(-\frac{1}{2}I - D + N \right) \mu.$$

Notably, the integral operator is full rank in this setting, and we do not have to augment the system.

- The double layer potential is now

$$D\mu := - \int_{\Gamma} \frac{1}{2\pi} \frac{(x-y) \cdot n(x)}{(x-y) \cdot (x-y)} \mu(y) dy.$$

We create a starfish outer boundary via cubic spline interpolation with 20 prescribed spline knots. For the interior holes, we use starfishes that are 16% the size of the outer boundary. We consider positions of the interior holes that lie along a path which is equal to a scaled-down version of the outer boundary. As each hole moves along this path, it is parametrized by the periodic variable $\theta_i \in [0, 2\pi)$. To prevent the holes from overlapping, we require that the distance between θ_1 and θ_2 (modulo 2π) be greater than $\pi/4$.

For the objective function, we estimate the derivative of the solution in the x -direction at the center of the domain, and try to find (θ_1, θ_2) which maximizes its value (see Figure 10 for a visualization of this function). We choose updates to (θ_1, θ_2) via gradient descent, where the gradient of the objective function is estimated by the fourth-order centered finite difference approximation. In other settings, more sophisticated techniques of analytically or numerically computing the gradients may be more appropriate, see [9, 21]. We choose the length of our descent step via a backtracking line-search. Hence, at each optimization step, we require the solution at a minimum of eight distinct but closely related geometries.

As discussed in Section 2.7, the factorization updates are less parallelizeable than the initial factorization. Instead of using multiple processors per factorization update, we can take advantage of them by computing the updates in parallel. As a result, the performance gain from using the updating scheme in an optimization setting is even greater than in Table 1 on a per-step measure (see Fig. 11).

Initializing the interior holes to be relatively far from their seemingly optimal positions, we see (Figure 12, left) rapid convergence to a local maximum. The value of (θ_1, θ_2) at the computed maximum matches that of the maximum seen in the center of Figure 10, top, and aligns with the intuitive expectation that the horizontal temperature gradient at the center of the domain is maximized by placing the heat source and sink on the left and right of the center.

4.3.2. Optimizing fluid source/sink placement. In this experiment (visualized in Fig. 9), we return to the Stokes equations and reuse the boundary from the previous experiment. Now the boundary conditions are:

- The outer boundary has unit-length horizontal flow to the right.
- One interior hole has unit-length normal flow out of the domain (acting as a sink), and the other has unit-length normal flow into the domain (acting as a source).

As our objective, we aim to maximize the horizontal flow to the left at the center of the domain. This choice yields interesting effects, as illustrated in Fig. 10, bottom—besides acting as fluid sources and sinks, the interior holes serve to obstruct the horizontal flow coming from the outer boundary. As a result, we see greater complexity in the dependence of the objective function on (θ_1, θ_2) . As in the previous

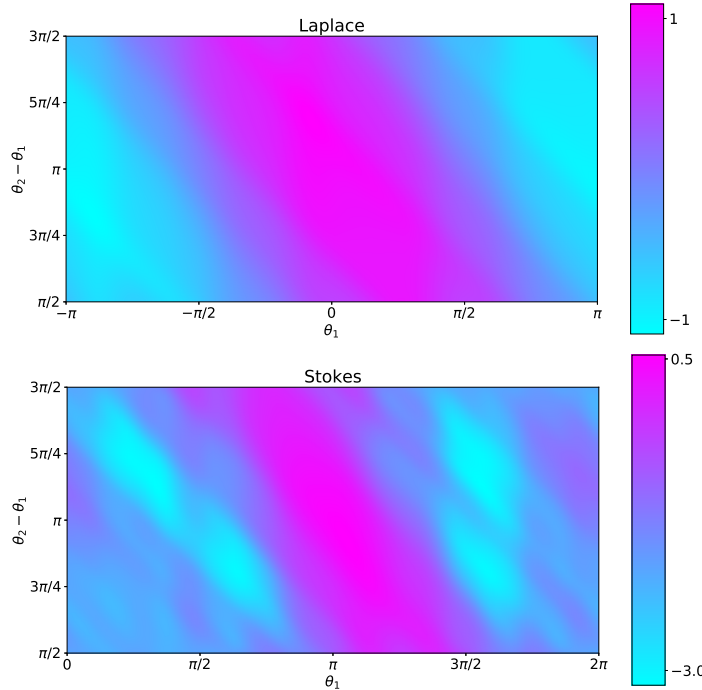


FIG. 10. Objective function value for 2,500 inner hole parameter pairs (θ_1, θ_2) . Note that while each plot seems to exhibit a good local maximum near the center, the landscape for Stokes flow is more complex, containing many local maxima. For these plots, we discretize the boundary using 4,096 integration nodes.

experiment, we see performance gains by efficient allocation of work among the four processors (Figure 11, right) and rapid convergence to a local maximum (Figure 12, left).

5. Conclusions. In this paper, we have demonstrated the applicability of skeletonization factorizations amenable to fast updating in solving large numbers of related boundary value problems. This can occur, for example, in geometry optimization or time dependent problems. Furthermore, we developed a general approach to solving problems where the kernel discretization is only a subblock of the whole system. This occurs, for example, when the domain is multiply-connected, and the relevant integral operators contain non-trivial null-spaces. The efficiency and parallelizability of our routines show great promise in areas where kernel matrices need to be factored multiple times following small updates to the underlying data points. Relevant areas include Gaussian process problems [29, 1], unsteady fluid simulations [3], and shape optimization of elastic structures [31].

While we take one specific approach to selecting skeleton points during compression, other methods may allow for greater parallelism between levels and reduce the number of computations needed to handle geometric perturbations.

Since the updating strategy currently relies on the locality of perturbations for its efficiency, further work in this area should include improving techniques for global geometry updates so that, *e.g.*, gradient-based optimization routines do not suffer from updating the entire boundary between steps. This may require a fundamental

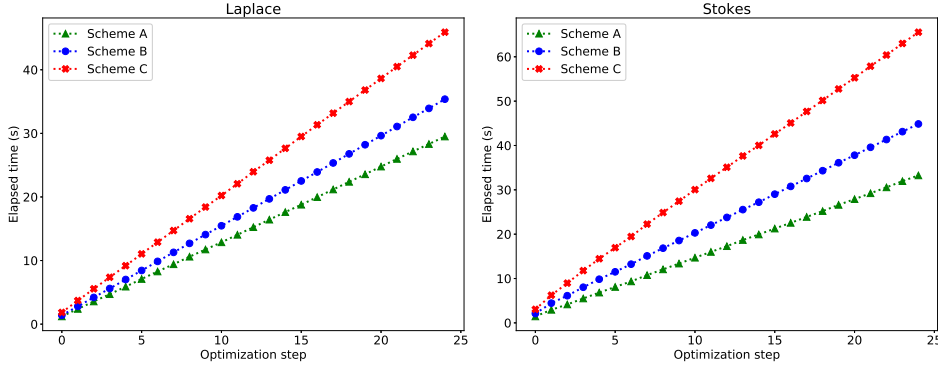


FIG. 11. Elapsed times of the optimization experiment described in Section 4.3.1 when using three different schemes for allocating work amongst four processors. In Scheme A, the related factorizations in the finite difference gradient approximation are each computed by a single processor. In Scheme B, each factorization is computed by two processors working in parallel, hence at most two updates are computed simultaneously. In Scheme C, each factorization is computed by four processors working in parallel, hence no updates are computed simultaneously. We discretize the boundary using 32,768 and 4,096 integration nodes for the left and right plots, respectively.

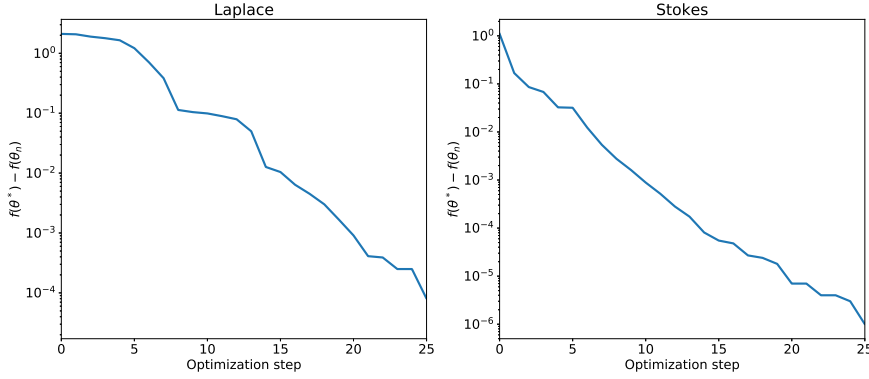


FIG. 12. Convergence to optimal configurations. The parameters found to maximize the objective functions match those predicted by Fig. 10. In the above convergence plots, the true optimal value $f(\theta^*)$ is approximated by allowing the optimization to run for a long time from an initial point based on Figure 10. As in Figure 11, we discretize the boundary using 32,768 and 4,096 integration nodes for the left and right plots, respectively.

change to the way leaf-level compression is performed and is the subject of ongoing work.

REFERENCES

- [1] S. AMBIKASARAN, D. FOREMAN-MACKEY, L. GREENGARD, D. W. HOGG, AND M. ONEIL, *Fast direct methods for gaussian processes*, IEEE Transactions on Pattern Analysis and Machine Intelligence, 38 (2016), pp. 252–265, <https://doi.org/10.1109/TPAMI.2015.2448083>.
- [2] M. BEBENDORF, *Hierarchical matrices*, Springer, 2008.
- [3] G. BIROS, L. YING, AND D. ZORIN, *An embedded boundary integral solver for the unsteady incompressible Navier-Stokes equations: Technical report*, NYU, 2001.
- [4] G. BIROS, L. YING, AND D. ZORIN, *A fast solver for the stokes equations with distributed forces in complex geometries*, Journal of Computational Physics, 193 (2004), pp. 317 –

- 348, <https://doi.org/https://doi.org/10.1016/j.jcp.2003.08.011>, <http://www.sciencedirect.com/science/article/pii/S0021999103004352>.
- [5] S. BÖRM, L. GASEDYCK, AND W. HACKBUSCH, *Introduction to hierarchical matrices with applications*, Engineering analysis with boundary elements, 27 (2003), pp. 405–422.
 - [6] H. CHENG, Z. GIMBUTAS, P.-G. MARTINSSON, AND V. ROKHLIN, *On the compression of low rank matrices*, SIAM Journal on Scientific Computing, 26 (2005), pp. 1389–1404.
 - [7] E. CORONA, P.-G. MARTINSSON, AND D. ZORIN, *An $O(N)$ direct solver for integral equations on the plane*, Applied and Computational Harmonic Analysis, 38 (2015), pp. 284 – 317, <https://doi.org/http://dx.doi.org/10.1016/j.acha.2014.04.002>, <http://www.sciencedirect.com/science/article/pii/S1063520314000529>.
 - [8] P. COULIER, H. POURANSARI, AND E. DARVE, *The inverse fast multipole method: Using a fast approximate direct solver as a preconditioner for dense linear systems*, SIAM Journal on Scientific Computing, 39 (2017), pp. A761–A796, <https://doi.org/10.1137/15M1034477>, <https://doi.org/10.1137/15M1034477>, <https://arxiv.org/abs/https://doi.org/10.1137/15M1034477>.
 - [9] M. B. GILES AND N. A. PIERCE, *An introduction to the adjoint approach to design*, Flow, Turbulence and Combustion, 65 (2000), pp. 393–415.
 - [10] A. GILLMAN, *Fast Direct Solvers for Elliptic Partial Differential Equations*, PhD thesis, Department of Applied Mathematics, University of Colorado at Boulder, 2011.
 - [11] A. GILLMAN, P. YOUNG, AND P.-G. MARTINSSON, *A direct solver with $O(N)$ complexity for integral equations on one-dimensional domains*, Frontiers of Mathematics in China, 7 (2012), pp. 217–247, <https://doi.org/10.1007/s11464-012-0188-3>, <http://dx.doi.org/10.1007/s11464-012-0188-3>.
 - [12] G. GOLUB, *Numerical methods for solving linear least squares problems*, Numer. Math., 7 (1965), p. 206216, <https://doi.org/10.1007/BF01436075>, <https://doi.org/10.1007/BF01436075>.
 - [13] L. GREENGARD, D. GUEYFFIER, P.-G. MARTINSSON, AND V. ROKHLIN, *Fast direct solvers for integral equations in complex three-dimensional domains*, Acta Numerica, 18 (2009), pp. 243–275, <https://doi.org/10.1017/S0962492906410011>, <http://journals.cambridge.org/article.S0962492906410011>.
 - [14] L. GREENGARD, S. JIANG, AND J. WANG, *On the accurate evaluation of unsteady stokes layer potentials in moving two-dimensional geometries*, arXiv preprint arXiv:1811.01840, (2018).
 - [15] L. GREENGARD AND V. ROKHLIN, *A fast algorithm for particle simulations*, Journal of computational physics, 73 (1987), pp. 325–348.
 - [16] W. HACKBUSCH, *Hierarchical matrices: algorithms and analysis*, vol. 49, Springer, 2015.
 - [17] K. HO AND L. GREENGARD, *A fast direct solver for structured linear systems by recursive skeletonization*, SIAM Journal on Scientific Computing, 34 (2012), pp. A2507–A2532, <https://doi.org/10.1137/120866683>, <http://dx.doi.org/10.1137/120866683>, <https://arxiv.org/abs/http://dx.doi.org/10.1137/120866683>.
 - [18] K. HO AND L. YING, *Hierarchical interpolative factorization for elliptic operators: Integral equations*, Communications on Pure and Applied Mathematics, (2015), <https://doi.org/10.1002/cpa.21577>, <http://dx.doi.org/10.1002/cpa.21577>.
 - [19] K. L. HO AND L. YING, *Hierarchical interpolative factorization for elliptic operators: differential equations*, Communications on Pure and Applied Mathematics, 69 (2016), pp. 1415–1451.
 - [20] G. HSIAO AND W. WENDLAND, *Boundary Integral Equations*, Applied Mathematical Sciences, Springer Berlin Heidelberg, 2008, https://books.google.com/books?id=_Gy56YLIGXEC.
 - [21] A. JAMESON, *Aerodynamic design via control theory*, Journal of Scientific Computing, 3 (1988), <https://doi.org/10.1007/BF01061285>.
 - [22] A. KLÖCKNER, A. BARNETT, L. GREENGARD, AND M. O’NEIL, *Quadrature by expansion: A new method for the evaluation of layer potentials*, Journal of Computational Physics, 252 (2013), pp. 332 – 349, <https://doi.org/https://doi.org/10.1016/j.jcp.2013.06.027>, <http://www.sciencedirect.com/science/article/pii/S0021999113004579>.
 - [23] X. LIU, J. XIA, AND M. V. DE HOOP, *Fast factorization update for general elliptic equations under multiple coefficient updates*, SIAM J. Sci. Comput., under revision, Purdue CCAM Report CCAM-2018-3, <http://ccam.math.purdue.edu/php-scripts/download> preprint. php/locupd. pdf, (2018).
 - [24] P.-G. MARTINSSON, *A fast direct solver for a class of elliptic partial differential equations*, Journal of Scientific Computing, 38 (2009), pp. 316–330, <https://doi.org/10.1007/s10915-008-9240-6>, <http://dx.doi.org/10.1007/s10915-008-9240-6>.
 - [25] P.-G. MARTINSSON, *Fast Direct Solvers for Elliptic PDEs*, Society for Industrial and Applied Mathematics, Philadelphia, PA, 2019, <https://doi.org/10.1137/1.9781611976045>,

- <https://epubs.siam.org/doi/abs/10.1137/1.9781611976045>, <https://arxiv.org/abs/https://epubs.siam.org/doi/pdf/10.1137/1.9781611976045>.
- [26] P.-G. MARTINSSON AND V. ROKHLIN, *A fast direct solver for boundary integral equations in two dimensions*, J. Comput. Phys., 205 (2005), pp. 1–23, <https://doi.org/10.1016/j.jcp.2004.10.033>, <http://dx.doi.org/10.1016/j.jcp.2004.10.033>.
 - [27] P.-G. MARTINSSON AND V. ROKHLIN, *An accelerated kernel-independent fast multipole method in one dimension*, SIAM Journal on Scientific Computing, 29 (2007), pp. 1160–1178, <https://doi.org/10.1137/060662253>, <http://dx.doi.org/10.1137/060662253>, <https://arxiv.org/abs/http://dx.doi.org/10.1137/060662253>.
 - [28] V. MINDEN, A. DAMLE, K. L. HO, AND L. YING, *A technique for updating hierarchical skeletonization-based factorizations of integral operators*, Multiscale Modeling & Simulation, 14 (2016), pp. 42–64, <https://doi.org/10.1137/15M1024500>, <http://dx.doi.org/10.1137/15M1024500>, <https://arxiv.org/abs/http://dx.doi.org/10.1137/15M1024500>.
 - [29] V. MINDEN, A. DAMLE, K. L. HO, AND L. YING, *Fast spatial gaussian process maximum likelihood estimation via skeletonization factorizations*, Multiscale Modeling & Simulation, 15 (2017), p. 15841611, <https://doi.org/10.1137/17m1116477>, <http://dx.doi.org/10.1137/17M1116477>.
 - [30] V. MINDEN, K. L. HO, A. DAMLE, AND L. YING, *A recursive skeletonization factorization based on strong admissibility*, Multiscale Modeling & Simulation, 15 (2017), p. 768796, <https://doi.org/10.1137/16m1095949>, <http://dx.doi.org/10.1137/16M1095949>.
 - [31] I. OSTANIN, D. ZORIN, AND I. OSELEDETS, *Parallel optimization with boundary elements and kernel independent fast multipole method*, International Journal of Computational Methods and Experimental Measurements, 5 (2017), pp. 154–162, <https://doi.org/10.2495/CMEM-V5-N2-154-162>.
 - [32] H. POWER, *The completed double layer boundary integral equation method for two-dimensional Stokes flow*, IMA Journal of Applied Mathematics, 51 (1993), pp. 123–145, <https://doi.org/10.1093/imamat/51.2.123>, <https://doi.org/10.1093/imamat/51.2.123>, <https://arxiv.org/abs/http://oup.prod.sis.lan/imamat/article-pdf/51/2/123/6765905/51-2-123.pdf>.
 - [33] Y. SAAD, *Iterative Methods for Sparse Linear Systems*, Society for Industrial and Applied Mathematics, second ed., 2003, <https://doi.org/10.1137/1.9780898718003>, <https://epubs.siam.org/doi/abs/10.1137/1.9780898718003>, <https://arxiv.org/abs/https://epubs.siam.org/doi/pdf/10.1137/1.9780898718003>.
 - [34] G. VAN DE VORST, *Integral method for the two-dimensional Stokes problem for multiply-connected domains applied to viscous sintering*, RANA : reports on applied and numerical analysis, Eindhoven University of Technology, 1992.
 - [35] S. K. VEERAPANENI, D. GUEYFFIER, D. ZORIN, AND G. BIROS, *A boundary integral method for simulating the dynamics of inextensible vesicles suspended in a viscous fluid in 2d*, Journal of Computational Physics, 228 (2009), pp. 2334 – 2353, <https://doi.org/https://doi.org/10.1016/j.jcp.2008.11.036>, <http://www.sciencedirect.com/science/article/pii/S0021999108006244>.
 - [36] S. K. VEERAPANENI, A. RAHIMIAN, G. BIROS, AND D. ZORIN, *A fast algorithm for simulating vesicle flows in three dimensions*, Journal of Computational Physics, 230 (2011), pp. 5610 – 5634, <https://doi.org/https://doi.org/10.1016/j.jcp.2011.03.045>, <http://www.sciencedirect.com/science/article/pii/S0021999111002063>.
 - [37] J. WANG, L. GREENGARD, S. JIANG, AND S. VEERAPANENI, *Fast integral equation methods for linear and semilinear heat equations in moving domains*, arXiv preprint arXiv:1910.00755, (2019).
 - [38] X. XING AND E. CHOW, *Interpolative decomposition via proxy points for kernel matrices*, SIAM Journal on Matrix Analysis and Applications, to appear, (2019).
 - [39] L. YING, G. BIROS, AND D. ZORIN, *A kernel-independent adaptive fast multipole algorithm in two and three dimensions*, Journal of Computational Physics, 196 (2004), pp. 591–626, <https://doi.org/10.1016/j.jcp.2003.11.021>, <http://dx.doi.org/10.1016/j.jcp.2003.11.021>.
 - [40] Y. ZHANG AND A. GILLMAN, *A fast direct solver for boundary value problems on locally perturbed geometries*, Journal of Computational Physics, 356 (2018), pp. 356–371.